Wake Effects in Lower Carbon Future Scenarios

Journal of Physics: Conference Series **2767** (2024) 092044 doi:10.1088/1742-6596/2767/9/092044

Wake Effects in Lower Carbon Future Scenarios

Julie K. Lundquist[1,2], **David J. Rosencrans**[2], **Owen Roberts**[1], **Anthony Lopez**[1], **Trieu Mai**[1]

[1] National Renewable Energy Laboratory, Golden, CO, USA
[2] University of Colorado, Boulder, CO, USA

E-mail: Julie.Lundquist@colorado.edu

Abstract. In August 2022, the U.S. Congress passed the Inflation Reduction Act (IRA), which intended to accelerate U.S. decarbonization, clean energy manufacturing, and deployment of new power and end-use technologies. The National Renewable Energy Laboratory has examined possible scenarios for growth by 2050 resulting from the IRA and other emissions reduction drivers and defined several possible scenarios for large-scale wind deployment. These scenarios incorporate large clusters of turbines operating as wind farms grouped around existing or likely transmission lines which will result in wind farm wakes. Using a numerical weather prediction (NWP) model, we assess these wake effects in a domain in the U. S. Southern Great Plains for a representative year with four scenarios in order to validate the simulations, estimate the internal wake impact, and quantify the cluster wake effect. Herein, we present a validation of the "no wind farm" scenario and quantify the internal waking effect for the "ONE" wind farm scenario. Future work will use the "MID" scenario (more than 8000 turbines) and the "HI" scenario (more than 16,000 turbines) to quantify the effect of cluster wakes or inter-farm wakes on power production.

1. Introduction

In August 2022, the U.S. Congress passed the Inflation Reduction Act (IRA). This law intended to accelerate U.S. decarbonization, clean energy manufacturing, and deployment of new power and end-use technologies. Several possible scenarios for growth of wind energy deployment can result from the IRA and other emissions reduction drivers [1]. NREL has defined several possible scenarios for large-scale wind deployment. These scenarios respect limitations for development (i.e. no wind deployment in urban areas or protected lands) and constraints such as spacing of at least five rotor diameters between turbines, but the scenarios do incorporate large clusters of turbines operating as wind farms grouped around existing or likely transmission.

As clusters of wind turbines wind farms extract momentum from the atmosphere, they may generate "wake effects" (decreases in downwind wind speeds), which undermine downwind wind turbines' power generation. Depending on atmospheric conditions, wakes have been observed to extend 50 km downwind or further [2], suggesting that these cluster wake effects between wind farms should be considered in power systems modeling for lower carbon futures.

Wake effects exert stronger impacts during stably stratified conditions [3] because the low levels of turbulence promote persistent wakes over large regions or for long periods of time. However, despite stable stratification, if wind speeds are fast enough, in region 3 of a turbine's power curve, wakes may not impact the power production of downwind turbines because even the reduced wind speeds will be in region 3. Due to this dependence on atmospheric stability

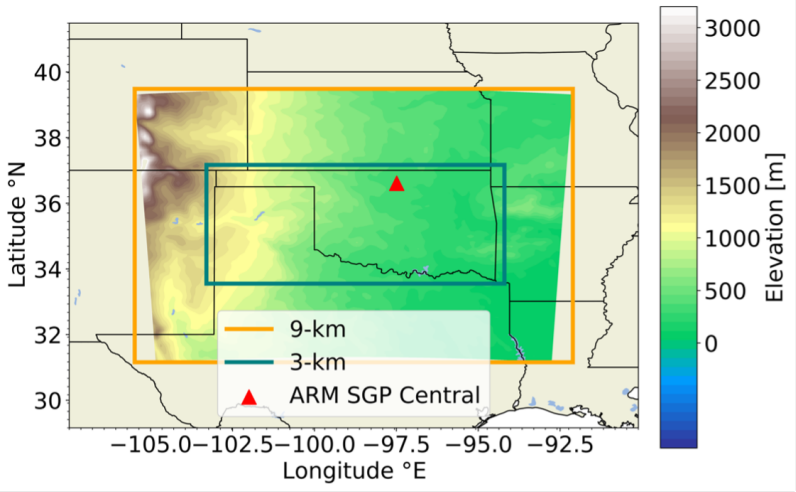

Figure 1. Simulation extent. Domains are outlined by rectangles with Domain 1 (orange) and Domain 2 (blue) and the ARM Southern Great Plains (SGP) central site (red triangle). Terrain elevation is shown as the colored contour.

and wind speed, empirical rules of thumb which quantify wake impacts can be imprecise, so atmospheric modeling provides a high-fidelity approach for cluster wake assessment. Numerical weather prediction (NWP) models can represent the wind speed reduction and enhanced turbulence in a cluster wake and resolve the spatio-temporal variability of cluster wake wind speed deficits and turbulence based on interactions with the atmosphere [4, 5, 6].

Herein, we use the Fitch wind farm parameterization (WFP) [4, 5] in the Weather Research and Forecasting (WRF) model to represent the effects of extensive wind energy deployment. We focus on a domain in the Southern Great Plains due to the strong and consistent wind resource as well as the availability of meteorological observations for evaluation of the simulations. This investigation explores two ambitious scenarios for wind development. Both scenarios have increased wind deployment in the region, but span a range of wind turbine densities to inform how wake effects might change with increasing wind turbine deployment. Before the results of these scenarios are assessed, we first evaluate the performance of the model by comparing simulations with the existing wind farm deployment to instrumentation deployed in this region. We also use a simulation with one wind farm to assess the internal waking effect. This paper presents the modeling set-up and scenario in Section 2 as well as the details of the validation in Section 3. Selected highlights of the results for future scenarios, focused on the internal waking effect, are briefly summarized in Section 4.

2. Model Set-up and Scenario

2.1. WRF modeling setup

We execute numerical weather prediction simulations using version 4.2.1 of the WRF model [7]. Our simulation domain focuses on a region with large current and planned wind energy deployment and extensive observational data for model validation (Fig. 1). A 9 km outer domain encompasses the Southern Great Plains, with a 3 km nested domain targeting Oklahoma and the Texas Panhandle region. Note that the effective resolution of the model is roughly 7 times coarser than the grid resolution [8]. Our modeling configuration includes a 10 min output frequency in the innermost domain, an 18 s timestep for the outer domain, and monthly reinitializations with two days of spin-up. We choose 10 m vertical grid resolution near the surface with stretching aloft. This setup includes 58 total levels which reach a 50 hPa top.

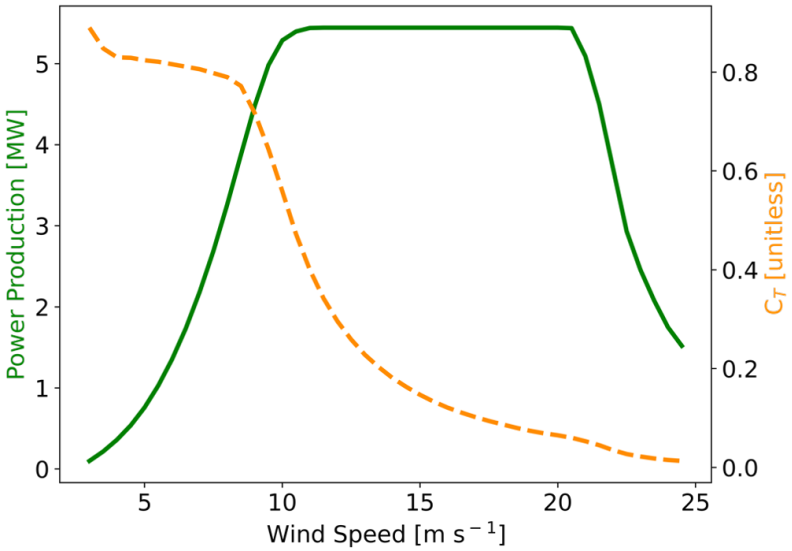

Figure 2. Characteristics of the 5.44 MW turbine with power production (green) and thrust coefficients (orange dashed) along the y-axis and wind speed across the x-axis.

Hourly, 0.25 deg x 0.25 deg initial and boundary conditions are supplied by the European Centre for Medium-Range Forecasts (ECMWF) fifth-generation reanalysis (ERA5) data set [9]. WRF physics and dynamics options are selected following a range of studies with primary focus on the SGP region [10, 3, 11, 12, 13, 14]. We choose the Mellor-Yamada Nakanishi and Nino (MYNN) Level 2.5 planetary boundary layer scheme with TKE advection turned on, the MYNN surface layer scheme [15], the rapid radiative transfer model for shortwave and longwave radiation [16], the Kain-Fritsch cumulus scheme [17] in the outermost domain only, WRF Single-Moment 5 microphysics [18], and the Noah land surface model [19]. The MYNN planetary boundary layer scheme is one of two which are compatible with the Fitch WFP [20, 21]. For the simulations with wind turbines, we use 100% of the possible TKE.

2.2. Turbine characteristics: future deployment

While actual wind energy deployment usually consists of a mix of different turbine types, for these idealized simulations we assume one type of turbine will be deployed throughout the domain. We select a turbine based on a Moderate Scenario of future technology advancement from Gagnon et al. [1]. This scenario predicts a representative onshore turbine with a 120 m hub height, 175 m rotor diameter, a specific power of 229 W m^{-2}, and a nameplate rating of 5.5 MW. To maintain a 175 m rotor diameter and 120 m hub height, we scale the power and thrust curves from the Vestas V150 4.0 MW turbine with a specific power of 220 W m^{-2}.

Power and thrust curves depend on the air density, which we estimate at the center of the domain (576.7 meters above sea level) to be 1.15 kg m^{-3} using a standard atmosphere. Power production increases from the cut-in wind speed (3 m s^{-1}) to the rated wind speed (11 m s^{-1}) and remains constant until the high-decibel threshold (20 m s^{-1}) (Figure 2). At wind speeds faster than this high-decibel threshold, power production decreases approaching the cut-out wind speed (24.5 m s^{-1}). Reduced thrust coefficients between the high-decibel and cut-out wind speeds mimic turbine rotors curtailing to reduce noise levels in populated regions.

2.3. Turbine characteristics: current deployment
The set of simulations compared to observed wind profiles during our selected year (2017 as discussed below) used locations, ratings, turbine hub-heights, and turbine rotor diameters of actual turbine deployments [22] with a normalized power curve.

2.4. Wind plant layouts
We site wind turbine locations for MID and HI growth scenarios [1] using the Renewable Energy Potential Model (reV) [23]. In the reV model, valid turbine coordinates are subject to exclusions such as land use, grid infrastructure, and a minimum of 5 rotor diameter spacing between turbines. These criteria result in two separate layouts (Table 1) consisting of 16,532 turbines and 8,592 turbines for the HI and MID growth scenarios, respectively. We further include a single wind plant (ONE) consisting of 257 turbines which allows us to distinguish between internal and external wake effects. The ONE plant is chosen for a located in the center of the domain and for being surrounded by upwind neighbors at most wind directions. The NWF scenario is used for assessing atmospheric stability, while the CWF scenario is used for model validation.

Table 1. Simulation details categorized by turbine specifications. All simulations run from 1 Jan 2017 - 31 Dec 2017. The "varied" turbines for the Current Wind Farm Simulation are taken from the USGS Wind Turbine database for the turbines deployed by 1 Jan 2017.

Simulation Type	Simulation Label	Turbine Type	# Turbines
No Wind Farms	NWF	N/A	0
Current Wind Farms	CWF	Varied (1-3.3 MW)	7175
One Wind Farm	ONE	5.44 MW	257
Medium Buildout	MID	5.44 MW	8592
High Buildout	HI	5.44 MW	16532

2.5. Year of investigation
We choose a representative modeling year based on turbine capacity factor. We use the renewables.ninja model [24, 25] to obtain the hourly wind power produced by a General Electric 2.5 MW xl wind turbine. This model incorporates 85 m hub-height wind speeds at the model grid cell housing the Atmospheric Radiation Measurement Southern Great Plains (ARM SGP) Central Facility coordinates (Fig. 3) from the Modern-Era Retrospective Analysis 2.0 (MERRA2) reanalysis product [26]. We divide the resulting hourly power production by the total possible 2.5 MW production at each hour from 2009 to 2020 (Figure 3). The average capacity factor of 44.3 % for the 11-year period is closest to the annual average capacity factor of 44.2% in 2017. Thus, we chose 2017 as a representative modeling year.

2.6. Atmospheric stability assessment
Atmospheric stratification affects the interaction of the wake with the larger atmosphere. Stable conditions with low ambient turbulence suppress vertical motion and limit wake wind speed recovery. Stable conditions tend to dominate during nocturnal hours. Unstable conditions tend to dominate during the day. These conditions are usually accompanied by larger values of turbulence, driven by buoyant convection. This ambient turbulence promotes wake wind speed recovery. We calculate the Obukhov length [27] L which dictates the height at which buoyant production of turbulence equals mechanical shear production of turbulence.

Figure 3. Annual Capacity Factor of a 2.5 MW turbine at the locating of the ARM Central Facility based on MERRA-2 data.

$$L = -\frac{u_*^3 \overline{\theta_v}}{\kappa g(\overline{w'\theta_v'})} \tag{1}$$

where u_* is the friction velocity, θ_v is the virtual potential temperature, κ is the von Kármán constant of 0.4, g is gravitational acceleration, and $\overline{w'\theta_v'}$ is the vertical turbulent surface heat flux. Following [28], values between 0 m and 1000 m are considered stably stratified, and values from -1000 m to 0 m are considered unstable. Values outside of this range are considered neutral. While L^{-1} (referred to as RMOL) is a direct output from WRF simulations, we instead calculate L using Equation 1 and WRF output values of UST (friction velocity) and HFX (surface heat flux) as these fluxes are used directly by the planetary boundary layer scheme.

3. Assessment of NWF and Validation of CWF simulations

This section addresses the simulations using the deployment of turbines as they were at the beginning of 2017.

3.1. Atmospheric stability assessment (NSF scenario)

As would be expected in an onshore situation, stratification in the NWF simulations exhibits both seasonal and diurnal variability. For a point at the center of the domain, unstable, stable, and neutral stratification occur 40.9%, 51.3%, and 7.8%, of the time, respectively . The predominance of unstable stratification is greatest in July, reaching 54.7% of the time (Figure 4a). In the northern hemisphere, days are longer during the summer months and incoming solar radiation reaches the surface at an angle more normal to the surface, causing stronger warming than in other seasons. While the longest day is June 21st, seasonal temperature lag extends the maximum occurrence of unstable conditions into July. The prevalence of stable conditions peaks in February, reaching 60.4% (Figure 4b), as incoming solar radiation reaches the surface at a shallower angle and the days are shorter. Neutral conditions occur most frequently during the springtime transition in April, up to 17% of the time (Figure 4c). In each season, atmospheric stratification exhibits a strong diurnal cycle due to daytime solar heating and nocturnal cooling of the surface. While rare, neutral stratification occurs during the early-morning (11-13 UTC) and evening hours (23-1 UTC) as surface heat flux approaches zero and changes sign.

3.2. Wind validation with lidar observations

We compare the simulated CWF wind speeds with meteorological observations from 2017 in the modeling domain. A scanning lidar at the ARM SGP Central Facility site makes measurements

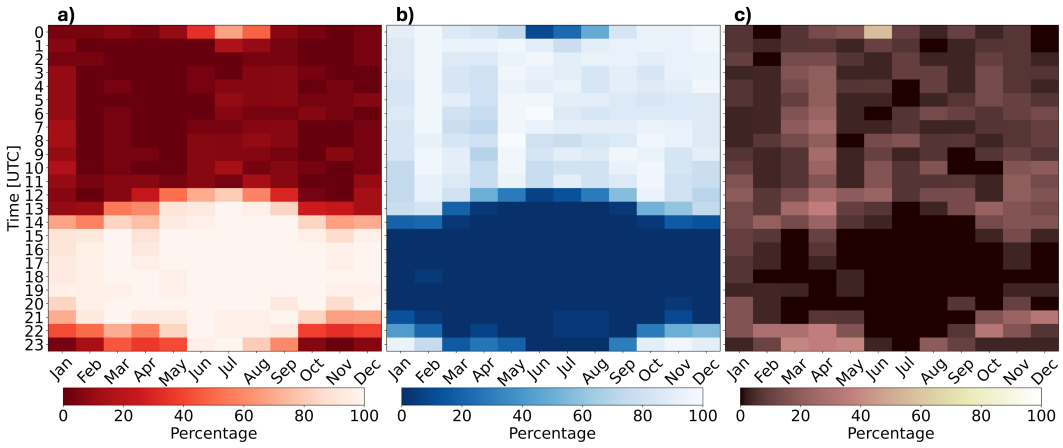

Figure 4. The percentages of occurrence of stability conditions as assessed by the Obukhov length from 01 January 2017 to 31 December 2017 at a point at the center of the domain. (a) unstable conditions, (b) stable conditions, and (c) neutral conditions. CST lags UTC by 6 hours.

of wind speeds at 15 min intervals. We compute wind velocity from lidar-returned radial velocity, azimuth, and elevation (above the horizon) angles following Frehlich et al. [29]. The elevation angle of Plan Position Indicator (PPI) lidar scans remains constant at 60 degrees. Thus, we select the 135 m range gate to assess wind speed measurements at 116 m, which is closest to the 120 m hub height. Only lidar radial velocity values with a quality control value of 0 are retained. Finally, we only consider lidar wind speeds between cut-in (3 m s^{-1}) and cut-out (24.5 s^{-1}) (Figure 2.

For comparison, we collect CWF wind speeds at the model grid cell that houses the ARM SGP Central site lidar. CWF hub-height wind speeds are vertically interpolated to the 116 m height and temporally interpolated to 15 min intervals to match the lidar output frequency. Any timestamps containing NaN values or in which the quality control value requires removal of lidar data are also removed from the CWF timeseries.

We verify model performance by calculating the correlation coefficient R, bias, and centered-root-mean-square error (cRMSE), as recommended for wind resource assessment by Optis et al. [30]:

$$r = \frac{\sum_i^N (V_{NWF_i} - \overline{V_{NWF}})(V_{lidar_i} - \overline{V_{lidar}})}{N \sigma_{NWF} \sigma_{lidar}} \tag{2}$$

$$Bias = \frac{\sum_i^N (V_{NWF_i} - V_{lidar_i})}{N} \tag{3}$$

$$cRMSE = \sqrt{\frac{\sum_i^N (V_{NWF_i} - \overline{V_{NWF}}) - (V_{lidar_i} - \overline{V_{lidar}})}{N \sigma_{NWF} \sigma_{lidar}}} \tag{4}$$

where V is the horizontal wind speed, N is the timeseries length, and σ is a standard deviation for the relevant quantity. We further calculate the Earth Mover's Distance or the Wasserstein metric, which we obtain from the Python SciPy function [31]. A correlation coefficient of 1 (Eq. 2) indicates that lidar and NWF wind speed timeseries increase and decrease in synchronization. Negative bias (Eq. 3) signifies an underestimation of NWF wind speeds and positive bias signifies an overestimation. A cRMSE (Eq. 4) of 0 indicates that lidar versus NWF wind speeds, with model bias removed, lie on the 1:1 regression line. A cRMSE value greater than 0 represents

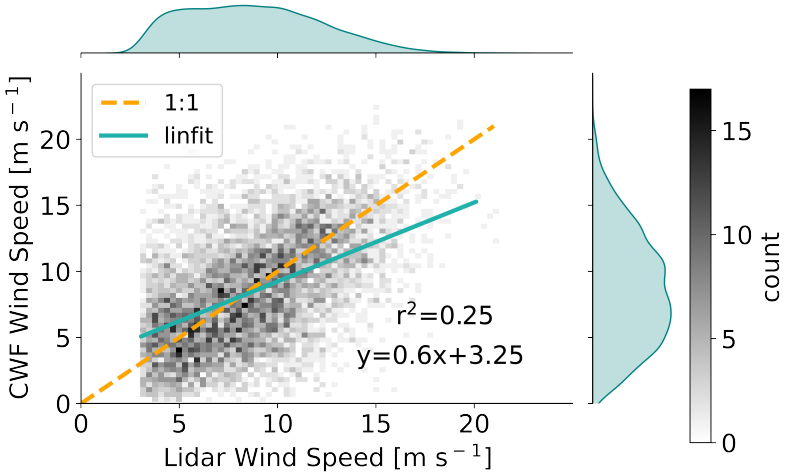

Figure 5. Modeled versus measured wind speeds between CWF and the ARM SGP Central lidar for the full year-long period from 01 Jan 2017 to 31 Dec 2017. The color contouring indicates the point density, the orange dashed line shows the 1:1 relationship, and the blue solid line shows the linear best fit. Blue shaded areas show the wind speed distributions

the distance of residual points from the regression line. The smaller the value of the EMD, the closer the agreement between the two populations.

Validation results suggest that the CWF simulations may overestimate wake impacts, as assessed at 116 m at the ARM SGP Central Facility site. Over the full year from 01 January 2017 to 31 December 2017, the meancoefficient of determination, cRMSE, EMD, and bias are 0.5, 3.55 m s^{-1}, 0.96 m s^{-1}, and -0.15 m s^{-1}, respectively. In general, CWF struggles to resolve wind speed ramps and sudden drops observed by the lidar which causes a low correlation coefficient. Bias is negative, suggesting an underestimation of wind speeds by CWF and overestimation of wake impacts. While no overestimation or underestimation would be preferable, the overestimation of wake impacts seen here suggests that wake impacts could also be overestimated in the MID and HIGH scenarios, thereby providing an upper bound of wake impacts for these future scenarios.

4. Results of future scenarios

Atmospheric stratification impacts the wake wind speed deficit. During unstable stratification where buoyant turbulence assists momentum entrainment into the wake, the mean wind speed reduction is smaller. Here, the maximum deficit in space reaches -0.75 m s^{-1} (Figure 6a). During stable stratification where vertical motion is suppressed, the maximum mean wake wind speed deficit increases to -1.31 m s^{-1} (Figure 6c). Over the full year-long period which accounts for both unstable and stable conditions, the maximum wake deficit in space reaches -1.05 m s^{-1} (Figure 6b).

Here we present only information on internal waking effect for the ONE simulation. Individual wind turbines generate internal wakes within the ONE wind plant that adversely impact electricity generation. To quantify internal wake effects at ONE, we first collect NWF wind speeds at the 120-m hub height in each grid cell containing ONE turbines. Wind speeds are convolved with the power curve and scaled by the number of turbines per cell, which returns the un-waked power production. Then, ONE power totals are divided by the NWF power estimations from the power curve. Again, each time stamp is categorized by hour of day and month of year, and percentages are binned for averaging. Finally, we calculate the total possible power production for use in capacity factor estimations by multiplying the total number of

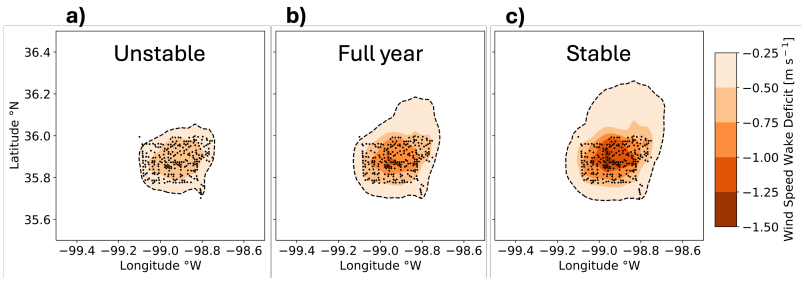

Figure 6. Average wake wind speeds for ONE during (a) unstable stratification, (b) the full year-long period, and (c) stable stratification. The wind speed deficit is shown by the color contouring and wind turbines as the black dots.

turbines by the nameplate rating of 5.44 MW. Over the year-long period, internal wakes from turbines within ONE cause a mean power loss of 11.45%.

5. Conclusions

The modeling study herein is designed to assess the wake impacts to surface meteorology and power production across the Southern Great Plains based on validated year-long simulations from 01 January 2017 to 31 December 2017 using the Weather Research and Forecasting (WRF) model. We execute a simulation without wind plants (NWF) and multiple simulations which incorporate the effects of wind turbines on the atmosphere (WFP). We explore the variability of results by including two future wind energy growth scenarios which feature medium (MID) and high (HI) amounts of capacity expansion. We discern between the internal and external effects of wakes on power generation by simulating one wind plant alone (ONE) and validate the model setup against lidar observations with a simulation of the atmosphere with wind turbines that exist as they did in 2017 (CWF).

Overall, we find fair agreement between CWF and lidar-measured wind speeds at 116 m with correlation coefficient, cRMSE, EMD, and bias values of 0.5, 3.55 m s^{-1}, 0.96 m s^{-1}, and -0.15 m s^{-1}, respectively. The CWF generally shows a negative bias, perhaps overestimating the reduction of wind speeds in wakes. The poor correlation coefficient suggests that the CWF simulations are unable to capture variability at this fine temporal resolution.

Atmospheric stratification in theNWF centered in the domain exhibits a strong diurnal cycle with a weaker seasonal pattern. Unstable conditions occur frequently during the daytime while stable conditions occur more often during the nocturnal and early morning hours. For the year-long period from 01 January 2017 to 31 December 2017, unstable, stable, and neutral stratification occur 40.9%, 51.3%, and 7.8% of the time, respectively.

The next stage in this research is to assess how the reduction of wind speeds in wakes limits the energy capture from wind turbine rotors. We will quantify the total wake-induced losses by comparing power production from the MID and HI scenarios to the power production based on convolving the NWF wind speeds with the wind turbine power curve. Further, using the ONE simulation as compared to the MID and HI simulations will distinguish the role of external wakes from internal wakes as in [32]. Internal wake losses likely will exceed external losses given the relatively close spacing between turbines, which limits the distance over which turbulence can replenish the wind speed. The results will inform grid operators, wind farm planners, and stakeholders by providing a predictable assessment of wake losses for plant- and grid-level management. The results will also inform national wind energy capacity expansion scenarios, illuminating potential costs or tradeoffs associated with regional wind plant clustering.

6. Acknowledgments

This work was authored in part by the National Renewable Energy Laboratory, operated by Alliance for Sustainable Energy, LLC, for the U.S. Department of Energy (DOE) under Contract No. DE-AC36-08GO28308. Funding provided by the U.S. Department of Energy Office of Energy Efficiency and Renewable Energy Wind Energy Technologies Office. The views expressed in the article do not necessarily represent the views of the DOE or the U.S. Government. The U.S. Government retains and the publisher, by accepting the article for publication, acknowledges that the U.S. Government retains a nonexclusive, paid-up, irrevocable, worldwide license to publish or reproduce the published form of this work, or allow others to do so, for U.S. Government purposes. The research was performed using computational resources sponsored by DOE and located at the National Renewable Energy Laboratory. This work utilized the Alpine and Blanca high performance computing resources at the University of Colorado Boulder. Alpine is jointly funded by the University of Colorado Boulder, the University of Colorado Anschutz, and Colorado State University. Blanca is jointly funded by computing users and the University of Colorado Boulder. Data storage supported by the University of Colorado Boulder 'PetaLibrary'.

References

[1] Gagnon P, Brown M, Steinberg D, Brown P, Awara S, Carag V, Cohen S, Cole W, Ho J, Inskeep S, Lee N, Mai T, Mowers M, Murphy C and Sergi B 2023 2022 Standard Scenarios Report: A U.S. Electricity Sector Outlook Tech. Rep. NREL/TP-6A40-84327 NREL Golden, CO

[2] Platis A, Bange J, Bärfuss K, Cañadillas B, Hundhausen M, Djath B, Lampert A, Schulz-Stellenfleth J, Siedersleben S, Neumann T and Emeis S 2020 *Meteorologische Zeitschrift* 355–376 ISSN , publisher: Schweizerbart'sche Verlagsbuchhandlung URL https://www.schweizerbart.de/papers/metz/detail/29/93565/Long_range_modifications_of_the_wind_field_by_offshore_wind_parks_results_of_the_project_WIPAFF

[3] Lundquist J K, DuVivier K K, Kaffine D and Tomaszewski J M 2019 *Nature Energy* **4** 26–34 ISSN 2058-7546 URL http://www.nature.com/articles/s41560-018-0281-2

[4] Fitch A C, Olson J B, Lundquist J K, Dudhia J, Gupta A K, Michalakes J and Barstad I 2012 *Monthly Weather Review* **140** 3017–3038 ISSN 1520-0493, 0027-0644 publisher: American Meteorological Society Section: Monthly Weather Review URL https://journals.ametsoc.org/view/journals/mwre/140/9/mwr-d-11-00352.1.xml

[5] Archer C L, Wu S, Ma Y and Jiménez P A 2020 *Monthly Weather Review* **148** 4823–4835 ISSN 1520-0493, 0027-0644 publisher: American Meteorological Society Section: Monthly Weather Review URL https://journals.ametsoc.org/view/journals/mwre/148/12/mwr-d-20-0097.1.xml

[6] Fischereit J, Brown R, Larsén X G, Badger J and Hawkes G 2022 *Boundary-Layer Meteorology* **182** 175–224 ISSN 1573-1472 URL https://doi.org/10.1007/s10546-021-00652-y

[7] Skamarock C, Klemp B, Dudhia J, Gill O, Liu Z, Berner J, Wang W, Powers G, Duda G, Barker D and Huang X y 2021 A Description of the Advanced Research WRF Model Version 4.3 Tech. Rep. NCAR/TN-556+STR URL https://opensky.ucar.edu/islandora/object/technotes%3A588/

[8] Skamarock W C 2004 *Monthly Weather Review* **132** 3019–3032 ISSN 0027-0644 URL https://journals.ametsoc.org/doi/full/10.1175/MWR2830.1

[9] Hersbach H, Bell B, Berrisford P, Hirahara S, Horányi A, Muñoz-Sabater J, Nicolas J, Peubey C, Radu R, Schepers D, Simmons A, Soci C, Abdalla S, Abellan X, Balsamo G, Bechtold P, Biavati G, Bidlot J, Bonavita M, Chiara G D, Dahlgren P, Dee D, Diamantakis M, Dragani R, Flemming J, Forbes R, Fuentes M, Geer A, Haimberger L, Healy S, Hogan R J, Hólm E, Janisková M, Keeley S, Laloyaux P, Lopez P, Lupu C, Radnoti G, Rosnay P d, Rozum I, Vamborg F, Villaume S and Thépaut J N 2020 *Quarterly Journal of the Royal Meteorological Society* **146** 1999–2049 ISSN 1477-870X _eprint: https://rmets.onlinelibrary.wiley.com/doi/pdf/10.1002/qj.3803 URL https://rmets.onlinelibrary.wiley.com/doi/abs/10.1002/qj.3803

[10] Lee J C Y and Lundquist J K 2017 *Geosci. Model Dev.* **10** 4229–4244 ISSN 1991-962X URL https://doi.org/10.5194/gmd-10-4229-2017

[11] Smith E N, Gebauer J G, Klein P M, Fedorovich E and Gibbs J A 2019 *Monthly Weather Review* **147** 1845–1869 ISSN 0027-0644, 1520-0493 URL http://journals.ametsoc.org/doi/10.1175/MWR-D-18-0293.1

[12] Tomaszewski J M and Lundquist J K 2020 *Geoscientific Model Development* **13** 2645–2662 ISSN 1991-959X publisher: Copernicus GmbH URL https://gmd.copernicus.org/articles/13/2645/2020/

[13] Bodini N, Lundquist J K and Moriarty P 2021 *Scientific Reports* **11** 22939 ISSN 2045-2322 number: 1 Publisher: Nature Publishing Group URL https://www.nature.com/articles/s41598-021-02089-2
[14] Sanchez Gomez M, Lundquist J K, Mirocha J D, Arthur R S, Muñoz-Esparza D and Robey R 2022 *Journal of Renewable and Sustainable Energy* **14** 063303 publisher: American Institute of Physics URL https://aip.scitation.org/doi/10.1063/5.0103668
[15] Nakanishi M and Niino H 2012 *Journal of the Atmospheric Sciences* **69** 3558–3575 ISSN 0022-4928 URL https://journals.ametsoc.org/doi/full/10.1175/JAS-D-11-0237.1
[16] Iacono M J, Delamere J S, Mlawer E J, Shephard M W, Clough S A and Collins W D 2008 *Journal of Geophysical Research: Atmospheres* **113**
[17] Kain J S 2004 *Journal of Applied Meteorology* **43** 170–181 ISSN 0894-8763 URL http://journals.ametsoc.org/doi/abs/10.1175/1520-0450%282004%29043%3C0170%3ATKCPAU%3E2.0.CO%3B2
[18] Hong S Y, Dudhia J and Chen S H 2004 *Monthly Weather Review* **132** 103–120 ISSN 0027-0644 URL http://journals.ametsoc.org/doi/abs/10.1175/1520-0493%282004%29132%3C0103%3AARATIM%3E2.0.CO%3B2
[19] Niu G Y, Yang Z L, Mitchell K E, Chen F, Ek M B, Barlage M, Kumar A, Manning K, Niyogi D, Rosero E, Tewari M and Xia Y 2011 *Journal of Geophysical Research: Atmospheres* **116** ISSN 2156-2202 _eprint: https://onlinelibrary.wiley.com/doi/pdf/10.1029/2010JD015139 URL https://onlinelibrary.wiley.com/doi/abs/10.1029/2010JD015139
[20] Juliano T W, Kosović B, Jiménez P A, Eghdami M, Haupt S E and Martilli A 2021 *Monthly Weather Review* **-1** ISSN 1520-0493, 0027-0644 publisher: American Meteorological Society Section: Monthly Weather Review URL https://journals.ametsoc.org/view/journals/mwre/aop/MWR-D-21-0164.1/MWR-D-21-0164.1.xml
[21] Rybchuk A, Juliano T W, Lundquist J K, Rosencrans D, Bodini N and Optis M 2022 *Wind Energy Science* **7** 2085–2098 ISSN 2366-7443 publisher: Copernicus GmbH URL https://wes.copernicus.org/articles/7/2085/2022/
[22] Hoen B, Diffendorfer J, Rand J, Kramer L, Garrity C and Hunt H 2018 United States Wind Turbine Database v6.1 (November 28, 2023) URL https://eerscmap.usgs.gov/windfarm/
[23] Maclaurin G, Grue N, Lopez A, Heimiller D, Rossol M, Buster G and Williams T 2019 The Renewable Energy Potential (reV) Model: A Geospatial Platform for Technical Potential and Supply Curve Modeling Tech. Rep. NREL/TP-6A20-73067, 1563140, MainId:13369 URL https://www.osti.gov/servlets/purl/1563140/
[24] Pfenninger S and Staffell I 2016 *Energy* **114** 1251–1265 ISSN 0360-5442 URL https://www.sciencedirect.com/science/article/pii/S0360544216311744
[25] Staffell I and Pfenninger S 2016 *Energy* **114** 1224–1239
[26] Gelaro R, McCarty W, Suárez M J, Todling R, Molod A, Takacs L, Randles C A, Darmenov A, Bosilovich M G, Reichle R, Wargan K, Coy L, Cullather R, Draper C, Akella S, Buchard V, Conaty A, da Silva A M, Gu W, Kim G K, Koster R, Lucchesi R, Merkova D, Nielsen J E, Partyka G, Pawson S, Putman W, Rienecker M, Schubert S D, Sienkiewicz M and Zhao B 2017 *Journal of Climate* **30** 5419–5454 ISSN 0894-8755 publisher: American Meteorological Society URL https://journals.ametsoc.org/jcli/article/30/14/5419/97087/The-Modern-Era-Retrospective-Analysis-for-Research
[27] Monin A S and Obukhov A M 1954 *Tr. Akad. Nauk. SSSR Geophiz. Inst.* **24** 163–187 URL http://mcnaughty.com/keith/papers/Monin_and_Obukhov_1954.pdf
[28] Muñoz-Esparza D, Cañadillas B, Neumann T and van Beeck J 2012 *Journal of Renewable and Sustainable Energy* **4** 063136 ISSN 19417012 URL http://scitation.aip.org/content/aip/journal/jrse/4/6/10.1063/1.4769201
[29] Frehlich R, Meillier Y, Jensen M L, Balsley B and Sharman R 2006 *Journal of Applied Meteorology and Climatology* **45** 821–837 ISSN 1558-8424 URL http://journals.ametsoc.org/doi/abs/10.1175/JAM2368.1
[30] Optis M, Bodini N, Debnath M and Doubrawa P 2020 Best Practices for the Validation of U.S. Offshore Wind Resource Models Tech. Rep. NREL/TP–5000-78375, 1755697, MainId:32292 URL https://www.osti.gov/servlets/purl/1755697/
[31] Virtanen P, Gommers R, Oliphant T E, Haberland M, Reddy T, Cournapeau D, Burovski E, Peterson P, Weckesser W, Bright J, van der Walt S J, Brett M, Wilson J, Millman K J, Mayorov N, Nelson A R J, Jones E, Kern R, Larson E, Carey C J, Polat Feng Y, Moore E W, VanderPlas J, Laxalde D, Perktold J, Cimrman R, Henriksen I, Quintero E A, Harris C R, Archibald A M, Ribeiro A H, Pedregosa F and van Mulbregt P 2020 *Nature Methods* **17** 261–272 ISSN 1548-7105 number: 3 Publisher: Nature Publishing Group URL https://www.nature.com/articles/s41592-019-0686-2
[32] Rosencrans D, Lundquist J K, Optis M, Rybchuk A, Bodini N and Rossol M 2023 *Wind Energy Science Discussions* **2023** 1–39 URL https://wes.copernicus.org/preprints/wes-2023-38/